Live-Bed Scour at Submerged Weirs

Dawei Guan[1]; Bruce W. Melville, M.ASCE[2]; and Heide Friedrich[3]

Abstract: Weirs or bed sills are low-head hydraulic structures used for bed stabilization, raising upstream water level, and reducing flow velocity. During high-flow events, the weir is fully submerged in the river and scouring occurs both upstream and downstream of the weir. For a fully submerged weir, the scour mechanism around the weir is dependent on approach flow intensity (clear-water scour conditions or live-bed scour conditions) and flow regimes (surface-flow regime or impinging-jet regime) over the weir. The fast evolution of underwater mobile topographies and propagating bedforms increase the complexities of the scour process and the difficulties for scour measurement at the submerged weir under live-bed scour conditions. This paper develops a measurement and data-processing technique for the study of scour at submerged weirs under extreme measurement environments and investigates the scour process both upstream and downstream of submerged weirs under live-bed scour conditions. The experiments are carried out with uniform sediment in a tilting sediment recirculating flume. Different flow rates and weir heights are used. For all the tests, the flow upstream of the weir is subcritical. Bed elevation changes are measured in the approach flow reach and in the scour zones both upstream and downstream of the weir using a Seatek multiple transducers array (MTA) (SeaTek Instrumentation, Florida). The highly contaminated raw bed-elevation data are filtered. Scour depths and bedform characteristics are extracted in data postprocessing. During live-bed conditions, a scour-and-fill process occurs immediately upstream from the weir in response to periodic approaching bedforms. The influence of the flow regimes on the scour mechanism downstream of the weir is discussed. Based on dimensionless analysis and experimental data, equations for prediction of the scour depth at the weir are proposed.
DOI: **10.1061/(ASCE)HY.1943-7900.0000954.**

Author keywords: Scour; Submerged weir; Flow regime; Live-bed condition; Bedform.

Introduction

Weirs or bed sills are low-head hydraulic structures that span the full width of the channel, and whose purpose is limiting excessive bed degradation, promoting bed stabilization, raising upstream water level, and reducing flow velocity. However, in alluvial rivers their presence causes flow disturbances, which result in local scour and possible undermining of the structures themselves. Scour prediction equations for downstream scour have been proposed by researchers (Bormann and Julien 1991; Gaudio et al. 2000; Lenzi et al. 2003a, b; D'Agostino and Ferro 2004; Marion et al. 2004; Comiti et al. 2005; Ben Meftah and Mossa 2006; Marion et al. 2006; Pagliara and Kurdistani 2013). However, almost all these equations are developed for unsubmerged or partially submerged weirs or sills, downstream of which scouring is a result of free over fall plunging jets (or partially submerged impinging jets). Due to the challenging measurement environment, limited experimental work, studying the effect of upstream sediment supply on scouring at weirs or bed sills, has been carried out (Marion et al. 2006; Bhuiyan et al. 2009). In addition, no local scouring observations have been made for submerged weirs in conditions with propagating bedforms, which are likely to occur in alluvial rivers during flood events (Fig. 1).

For a fully submerged weir, flow regimes over the weir can be classified as: (1) surface jet, (2) surface wave, (3) breaking wave (or surface jump), and (4) impinging jet (Wu and Rajaratnam 1996). The first three regimes can be collectively named the surface-flow regime; for these, the flow remains as a jet at the surface in the downstream channel, with its thickness increasing downstream because of turbulent mixing. For the impinging-jet regime, the flow over the weir plunges into the tailwater, diffuses as a plane submerged jet, and eventually hits the bed of the downstream channel (Wu and Rajaratnam 1998). To date, studies on flow regime effects on the scouring process at weirlike structures are limited (Comiti and Lenzi 2006; Comiti et al. 2009).

Depending on the upstream sediment transport conditions, the local scour can be classified as either clear-water scour or live-bed scour. During clear-water scour, the sediment is slowly removed from the scour hole at the structure, but not replenished by the approach flow. During live-bed scour, the scour process becomes complex due to the sediment transport process at the structure. For live-bed scour at a submerged weir, scouring occurs both upstream and downstream of the weir. The bedforms propagate over the weir in the form of suspended load. The suspended load and the entrained air bubbles in the diffusing jets in the scour hole result in a challenging measurement environment. The locations of the maximum scour depth both upstream and downstream of the weir are continually shifting because of secondary flow effects and the irregular shapes of approaching bedforms. Thus, development of a technique for accurate extraction of the maximum scour depth around the weir is needed for live-bed conditions.

This paper aims to develop a measurement and data-processing technique for the study of scour at submerged weirs under extreme measurement environments and to investigate the scour process

[1]Ph.D. Student, Dept. of Civil and Environmental Engineering, Univ. of Auckland, Private Bag 92019, Auckland 1142, New Zealand (corresponding author). E-mail: dgua324@aucklanduni.ac.nz

[2]Professor, Dept. of Civil and Environmental Engineering, Univ. of Auckland, Private Bag 92019, Auckland 1142, New Zealand. E-mail: b.melville@auckland.ac.nz

[3]Lecturer, Dept. of Civil and Environmental Engineering, Univ. of Auckland, Private Bag 92019, Auckland 1142, New Zealand. E-mail: h.friedrich@auckland.ac.nz

Note. This manuscript was submitted on March 4, 2014; approved on September 10, 2014; published online on October 27, 2014. Discussion period open until March 27, 2015; separate discussions must be submitted for individual papers. This paper is part of the ***Journal of Hydraulic Engineering***, © ASCE, ISSN 0733-9429/04014071(12)/$25.00.

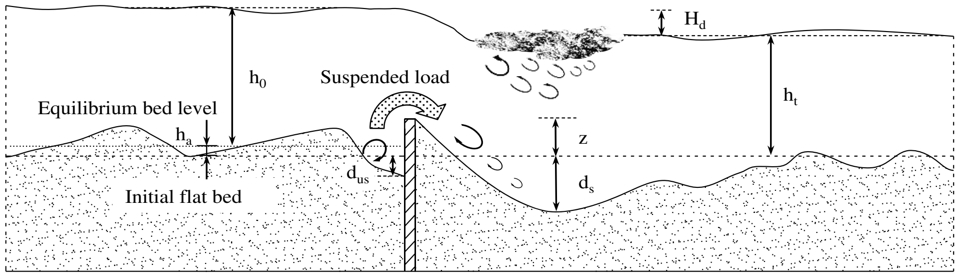

Fig. 1. Sketch of scouring at a submerged weir under the live-bed scour condition

both upstream and downstream of submerged weirs under live-bed scour conditions.

Experimental Setup and Methodology

Experimental Setup

The experiments were carried out in a tilting flume with a dimension of 12 m long, 0.44 m wide, and 0.58 m deep in the Fluid Mechanics Laboratory of the University of Auckland, New Zealand. The flume has a main pump and a sediment pump. The main pump circulates water and a small amount of suspended sediment. The speed of the main pump is controlled by a variable electronic speed control unit, while the sediment pump speed is set to a constant speed. At the upstream end of the flume, water and sediment are fed into a mixing chamber and enter the flume through a honeycomb flow straightener, which effectively eliminates any rotational flow component induced in the return pipelines. At the downstream end, bed load sediment is trapped in a separate hopperlike sump and pumped to the inlet by the sediment pump.

The sediment used in the experiments was coarse sand, for which the median diameter $d_{50} = 0.85$ mm and relative submerged particle density $\Delta = 1.65$. The sediment size distribution was near uniform, with a standard deviation $\sigma_g = 1.3$ ($d_{16} = 0.65$ mm, $d_{30} = 0.73$ mm, $d_{84} = 1.10$ mm, $d_{90} = 1.15$ mm). The submerged weirs were 10 mm-thick rectangular plastic plates, covering the width of the flume.

Throughout the experiment, the scour development at both sides of the weir, and the bed elevation changes in the approach flow, were measured as a function of time using a Seatek multiple transducer array (MTA). The apparatus is an ultrasonic ranging system, comprising 64 transducers, which instantaneously measures the distance to reflective objects under the water. The transducers have a precision of ± 1 mm. A detailed description of this device was given in Friedrich et al. (2005). The transducers were installed in straight metal tubes with a diameter of 14 mm, mounted to the top flume rail. The system was operated with 40 transducers at three frequencies (1, 2.44, and 3 Hz), depending on the scour rate. As seen in Fig. 2, Transducers $1 \sim 2$ were used for recording bed elevation changes in the approach flow, Transducers $3 \sim 5$ were used for recording the scour process upstream of the weir, Transducers $6 \sim 40$ were used for recording the scour process downstream of the weir.

Prior to starting the main test program, preliminary tests, covering the range of flow rates, were used to observe the live-bed scour process and locate the maximum scour depth on both sides of the weir. It was observed that upstream maximum scour depths occur immediately upstream from the weir, whereas downstream maximum scour depths shift within a certain zone; the location of the zone, which is shown hatched in Fig. 2, varied with flow intensity. The distance between the weir and the *hatched zone* ranged from 300 to 500 mm (Fig. 2).

For the clear-water scour tests, the scour process downstream of the weir is very slow and takes a long time to reach equilibrium, and the scour holes are relatively long. Therefore, instead of using stationary transducers to measure the maximum scour depth, a moving carriage with 25 transducers was used to obtain the clear-water scour bed profile of as a function of time. The detailed description of transducer arrangement and extraction of maximum scour depths is given in Guan et al. (2014).

During live-bed scour tests, the bedforms migrate along the flume and the sectional flow depth is continually changing; this significantly affects the accuracy of velocity measurements. Therefore, a flat fixed bed was used during calibration of the pump flow rates before any tests were carried out. During calibration, the tailwater depth in the flume sump and flume slope were the same as that of corresponding tests. The vertical velocity profiles were measured using a Nortek Vectrino+ (Nortek, Rud, Norway) and integrated to determine the flow rates for the corresponding pump speeds. During the tests, the averaged approach velocity, U_0, for each pump speed was determined from the calibrated flow rate and the approach averaged water depth, h_0. The corresponding critical average approach velocity, U_c, is calculated from the logarithmic form of the velocity profile $U_c/u_{*c} = 5.75 \log(5.53 h_0/d_{50})$, in which the average approach flow critical shear velocity $u_{*c} = 0.021$ m/s was determined

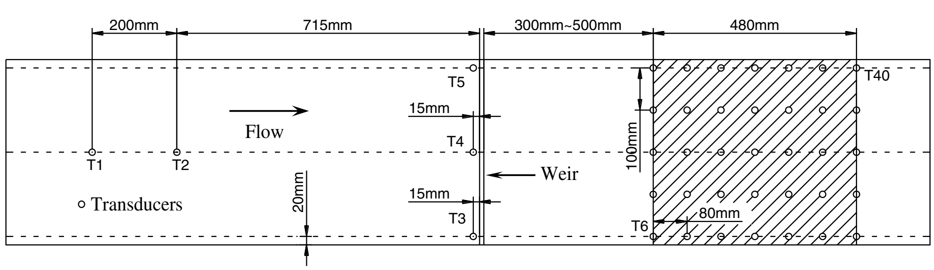

Fig. 2. Plan view of transducer arrangement for measuring bed elevation changes

using the Shields diagram for the respective particle size (Melville 1997). In this study, three weir heights, z (30, 40, 50 mm) were used and a total of 6 clear-water scour tests and 42 live-bed scour tests were carried out. For each weir height, the flowrate, Q, was systematically varied by applying the calibrated pump speeds, and the tailwater depth, h_t, was adjusted, at the beginning of the test, to normal depth by adjusting the flume slope and the level of the overflow pipe in the sump at the end of the flume. The tailwater depth (150 mm) was kept constant. The water level difference across the weir, H_d, was determined using the water surface profiles, which were measured using a point gage with a precision of ± 1 mm. The average approach flow depth, h_0, is calculated as $h_0 = h_t + H_d - h_a$, in which h_a is the average upstream aggradation height in the equilibrium stage. The upstream Froude number for all the tests varied in the range of 0.14 and 0.87. A summary of the experimental conditions is shown in Table 1. To optimize the amount of data obtained during the available time, a continuous experimental method was used to reduce the overall setup time. For each weir height, the higher velocity tests were a continuation of a previous lower velocity test; the flow velocity was increased at the end of the previous test to reach the equilibrium for the next velocity. The same method was used by Sheppard and Miller (2006).

Bed Topographical Data Preprocess

During all live-bed scour tests, bed elevation changes at the locations shown in Fig. 2 were continuously recorded by all 40 transducers. The measurement environments were very challenging because of the fast evolution of underwater mobile topographies. The raw data records are inevitably contaminated with noise from

Table 1. Summary of Experimental Conditions

Test number	Q (m^3/s)	z (mm)	H_d (mm)	h_t (mm)	h_0 (mm)	h_a (mm)	U_0 (m/s)	U_c (m/s)	Flume slope S (%)	F_u	t (h)
SCS4PO6.4	0.0122	30	0	150	150	0	0.185	0.367	0.042	0.15	1
SCS5PO12	0.0231	30	1	150	151	0	0.348	0.367	0.063	0.29	450
SLSP12	0.0310	30	5	150	150	5	0.469	0.367	0.084	0.39	65
NLS1P13	0.0337	30	5	150	152	3	0.504	0.367	0.116	0.41	23.9
NLS2P15	0.0374	30	6	150	154	2	0.552	0.368	0.147	0.45	23.9
NLS3P17	0.0418	30	8	150	154	4	0.616	0.368	0.168	0.50	19.4
NLS4P19	0.0466	30	10	150	156	4	0.679	0.369	0.211	0.55	17.1
NLS5P21	0.0503	30	12	150	157	5	0.728	0.369	0.242	0.59	12
NLS6P23	0.0540	30	14	150	159	5	0.772	0.370	0.284	0.62	9.2
NLS7P25	0.0583	30	16	150	160	6	0.829	0.370	0.326	0.66	8
NLS8P27	0.0622	30	19	150	161	8	0.877	0.370	0.389	0.70	4
NLS9P29	0.0659	30	21	150	161	10	0.930	0.370	0.432	0.74	2
SLSP31	0.0719	30	24	150	164	10	0.997	0.371	0.463	0.79	2
SLSP33	0.0773	30	28	150	167	11	1.053	0.372	0.516	0.82	2
SLSP35	0.0814	30	32	150	172	10	1.076	0.374	0.537	0.83	2
SLSP37	0.0860	30	36	150	175	11	1.117	0.375	0.568	0.85	1.5
SLSP39	0.0905	30	40	150	178	12	1.155	0.376	0.611	0.87	1.5
SCS0PO6	0.0115	40	0	150	150	0	0.174	0.367	0.042	0.14	1
SCS1P5.8	0.0199	40	1	150	151	0	0.300	0.367	0.053	0.25	600
SCS2P7.5	0.0230	40	2	150	152	0	0.343	0.367	0.063	0.28	600 + 164[a]
SLSP12	0.0310	40	8	150	149	9	0.472	0.366	0.084	0.39	83.3
NLS10P13	0.0337	40	9	150	151	8	0.507	0.367	0.116	0.42	45.5
NLS11P15	0.0374	40	10	150	153	7	0.556	0.368	0.147	0.45	27.7
NLS12P17	0.0418	40	12	150	155	7	0.612	0.368	0.168	0.50	21.8
NLS13P19	0.0466	40	15	150	158	7	0.670	0.369	0.211	0.54	18.2
NLS14P21	0.0503	40	17	150	159	8	0.719	0.370	0.242	0.58	15.9
NLS15P23	0.0540	40	19	150	161	8	0.762	0.370	0.284	0.61	10
NLS16P25	0.0583	40	23	150	163	10	0.814	0.371	0.326	0.64	8
NLS17P27	0.0622	40	26	150	162	14	0.872	0.371	0.389	0.69	4
SLSP29	0.0659	40	29	150	164	15	0.913	0.371	0.432	0.72	3.2
SLSP31	0.0719	40	34	150	168	16	0.973	0.373	0.463	0.76	1.8
SLSP33	0.0773	40	38	150	172	16	1.022	0.374	0.516	0.79	1.4
SLSP35	0.0814	40	43	150	176	17	1.052	0.375	0.537	0.80	1
SLSP37	0.0860	40	45	150	176	19	1.111	0.375	0.568	0.85	1
SCS5PO5.6	0.0107	50	0	150	150	0	0.162	0.367	0.042	0.13	1
SLS1P12	0.0310	50	12	150	145	17	0.485	0.365	0.084	0.41	96
NLS18P13	0.0337	50	13	150	148	15	0.518	0.366	0.116	0.43	45.5
NLS19P15	0.0374	50	15	150	154	11	0.552	0.368	0.147	0.45	34.1
NLS20P17	0.0418	50	18	150	155	13	0.612	0.368	0.168	0.50	20.5
NLS21P19	0.0466	50	22	150	160	12	0.662	0.370	0.211	0.53	17.1
NLS22P21	0.0503	50	25	150	161	14	0.710	0.370	0.242	0.56	12
NLS23P23	0.0540	50	28	150	163	15	0.753	0.371	0.284	0.60	12
SLS7P24	0.0557	50	31	150	161	20	0.788	0.370	0.305	0.63	12
NLS24P25	0.0583	50	33	150	161	22	0.824	0.370	0.326	0.66	7.7
NLS25P27	0.0622	50	36	150	164	22	0.861	0.371	0.389	0.68	3
SLS9P28	0.0639	50	39	150	165	24	0.881	0.372	0.421	0.69	2
SLS10P29	0.0659	50	41	150	165	26	0.908	0.372	0.442	0.71	1
SLS11P30	0.0687	50	43	150	166	27	0.941	0.372	0.474	0.74	1

[a]Clear-water scour test SCS2P7.5 is a continuation of test SCS1P5.8 (by increasing flow rate at the end of test SCS1P5.8).

various sources, such as reflections of suspended load or air bubbles, or instrumentation contact errors. The contamination levels vary for different flow rates and different measurement locations. If the absolute slope value between a good data point and the neighboring data point was larger than a certain threshold, the neighboring point was treated as an erroneous spike and given an interpolated value. In this study, because of the short time interval between two adjacent recorded points, 2 mm per time step was adopted as the threshold value. Friedrich (2010) used this technique in similarly challenging measurement environments. The filtering process of the raw time-series bed elevation data has the following steps:

1. Ensure that the first data point of a time-series dataset is a good data point; otherwise, start with the first point in the data series that is a good data point;
2. Calculate the absolute slope between the first data point and the next neighboring data point;
3. Determine if the maximum allowable slope is exceeded;
   (a). If the maximum allowable slope is exceeded, assume that the second data point is an outlier, calculate the slope between the first data point and the next neighboring data point, and go back to Step 3;
   (b). If the maximum allowable slope is not exceeded, adopt the second data point as a good point and set it as the new first data point, calculate the slope between the new first data point and the next neighboring data point, and go back to Step 3;
4. Replace the outlier data with linearly interpolated data between good data points; and
5. Conduct Steps $2 \sim 5$ for all data point of the time-series data set.

Fig. 3(a) shows an example of filtered data using the above method.

For most experimental conditions in this study, the above filtering method functions provides accurate bed profiles. However, the technique could not be applied for Transducers $3 \sim 5$ in very high flow rate conditions ($U_0 > 0.7$ m/s), which recorded the scour process upstream of the weir, the noisiest measurement location, resulting in extreme contamination levels (over 80% of data are contaminated). In this case, the boundary outline of bed elevation profiles has to be manually identified. Fig. 3(b) shows an example of manually filtered data. Comparison of manually filtered data with slope detection filtered data for Transducers $3 \sim 5$ at low flow rate tests showed a very small difference (less than 2%) in final extracted values of upstream average maximum scour depths.

Extraction of Bedform Characteristics and Scour Data

After preprocessing of the bed topographical data, the filtered time-series datasets $X_i(t)$ for transducer i ($i = 1 \sim 40$) were obtained with zero datum at the initial flat bed level. Upstream bedform characteristics and evolution of maximum scour depth both upstream and downstream of the weir can be extracted from $X_1(t) \sim X_{40}(t)$. The upstream aggradation height h_a is calculated as $h_a = E[X_1(t)]$.

Because of the short distance between Transducers 1 and 2, the migrating bedform maintains its geometry while passing below these two transducers. The bed elevation changes at any point between Transducers 1 and 2 on the centerline approximately follow a stationary random process. Therefore, the time delay Δt between $X_1(t)$ and $X_2(t)$ can be determined using the cross-correlation function $R_{x_1 x_2}$. An example of a cross-correlation result is shown in Fig. 4. The bedform celerity, c, can be calculated as $c = L/\Delta t$, in which L is the distance between Transducers 1 and 2.

The following steps are used for the quantification of bedform geometry in terms of average bedform height and period (see example in Fig. 5):

1. Extract the points $\{t(n), X_1[t(n)]\}$, where bedform crests and troughs pass Transducer 1, from the dataset $X_1(t)$, for which the number n must be even;

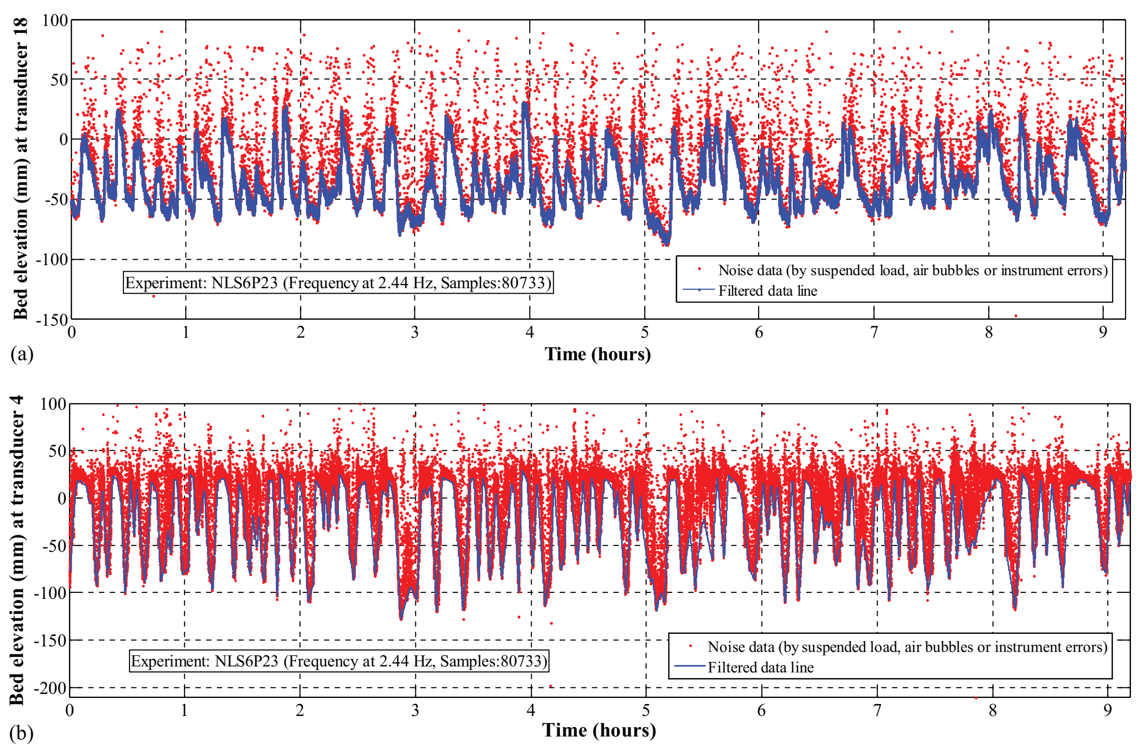

Fig. 3. (Color) Data filtering process: (a) slope detection filtering method; (b) manually filtered

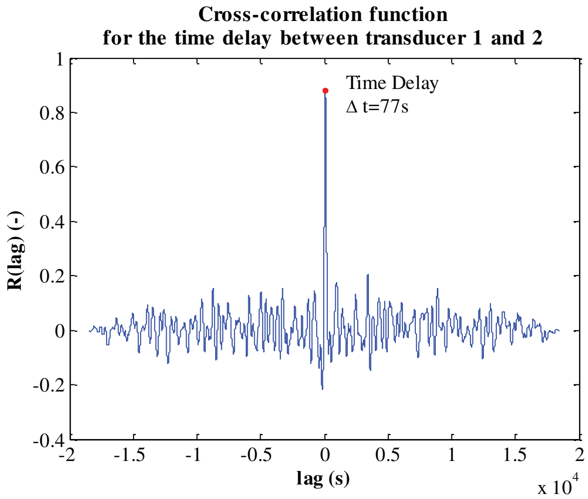

Fig. 4. (Color) Bedform cross-correlogram for test NLS6P23

2. Calculate serial bedform periods $t_p(m)$, $t_p(m) = t(2m+1) - t(2m-1)$, in which $m = n/2$;
3. Calculate serial bedform heights $\eta(m)$, $\eta(m) = |X_1[t(2m)] - X_1[t(2m-1)]|$;
4. Determine average bedform heights η, $\eta = E[\eta(m)]$ and average bedform period T, $T = E[t_p(m)]$; and
5. Determine average bedform length λ, $\lambda = cT$.

In this study, the bedform regime transition stage was observed when flow intensity (U_0/U_c) was greater than 3. However, because the sediment layer used in the flume was of limited thickness, scour depths reached the bottom of the flume before the upper bedform regime (plane bed and antidunes) was reached.

The location of the maximum scour depth upstream of the weir shifted in the frontal zone of the upstream face of the weir. This is due to the irregular shape of migrating bedforms. In this study, the measurement points were set on the centerline of the flume, near the side walls and immediately upstream of the weir (Fig. 2). Based on observations during preliminary live-bed scour tests, the maximum scour depths were known to frequently occur at those three locations. For each live-bed scour test, the evolution of maximum scour depth upstream of the weir, $d_{us}(t)$, was extracted from datasets $X_3(t) \sim X_5(t)$, where $d_{us}(t) = -M\text{in}[X_3(t) \sim X_5(t)]$. Fig. 6 shows an example of a time series of the scour process upstream of the weir.

As seen in Fig. 6, a scour-and-fill process occurs immediately upstream of the weir (for all live-bed scour tests). It was observed that the scour hole at the upstream base of the weir develops as a bedform trough approaches the weir, and reaches its maximum depth when the bedform trough arrives at the weir, then gradually fills as the next dune crest approaches.

The directly averaged value of the data series $d_{us}(t)$ was considered to be unsuitable as a scour parameter for the design of

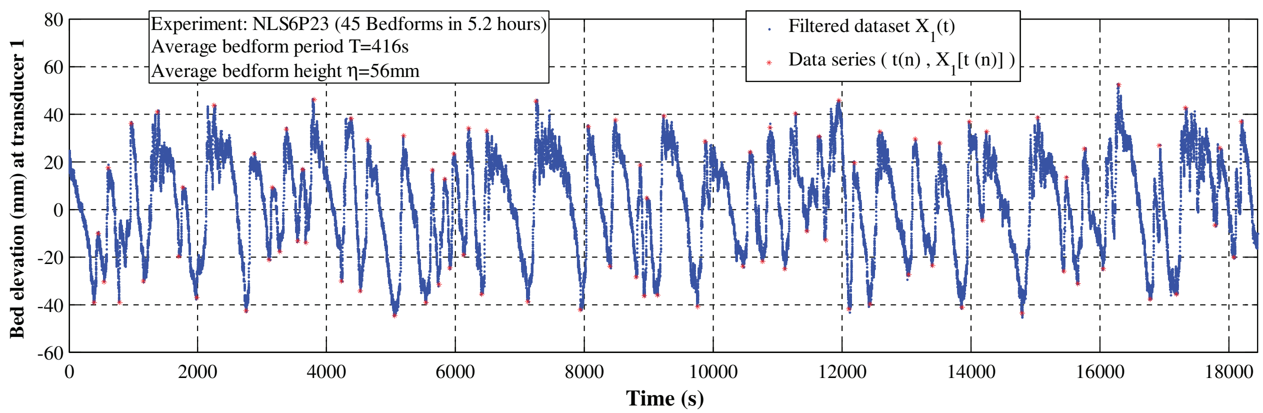

Fig. 5. (Color) Extraction of average bedform period and average bedform height

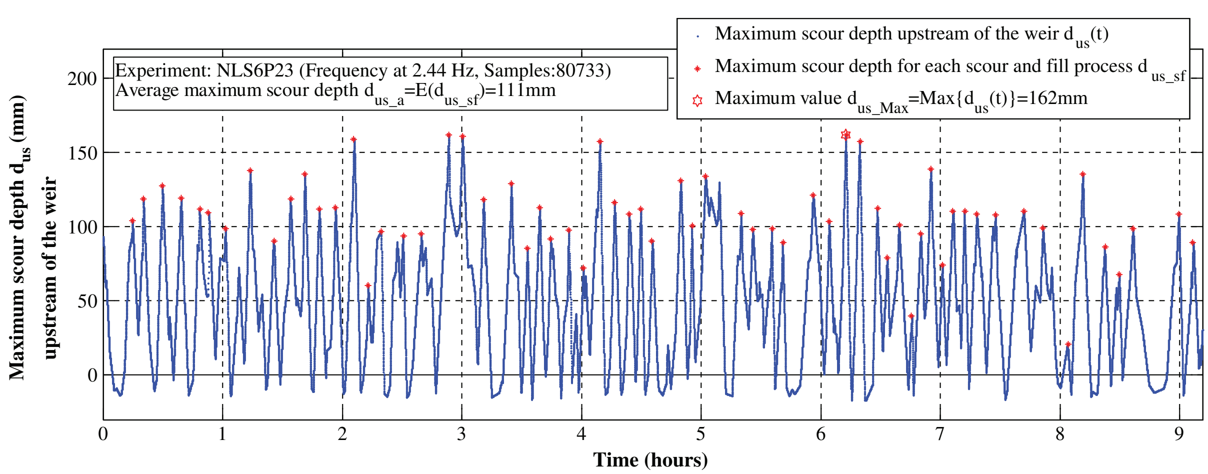

Fig. 6. (Color) Scour process upstream of the weir

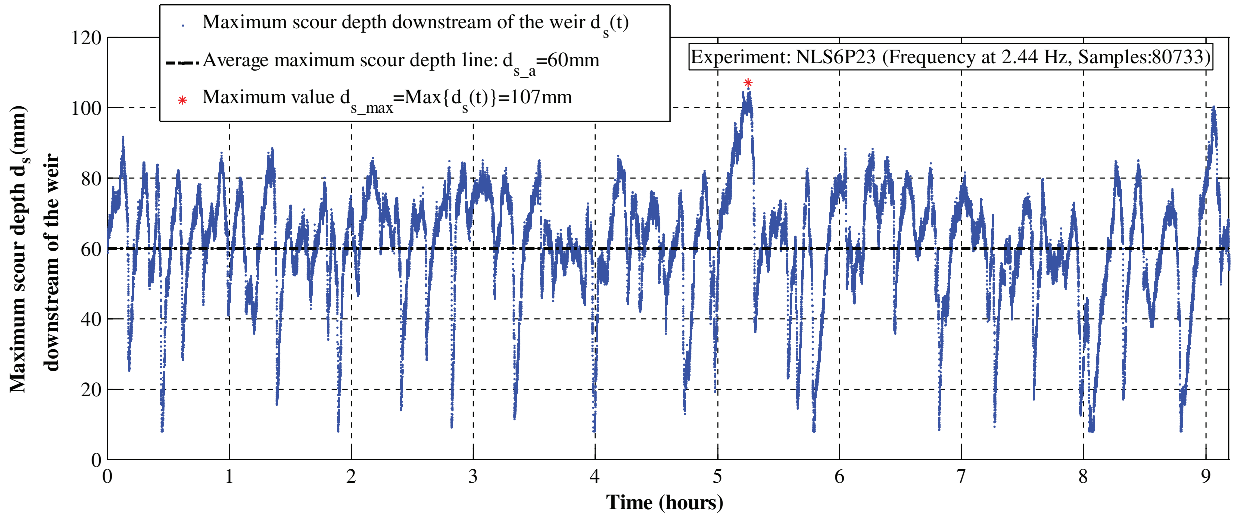

Fig. 7. (Color) Scour process downstream of the weir

upstream weir protection. Instead, the average value, d_{us_a}, of the maximum scour depths during each scour-and-fill cycle, d_{us_sf}, is used as the upstream scour parameter (Fig. 6). The average maximum scour depth, d_{us_a}, and the maximum value, $d_{us\_\max}$, were extracted from the data series $d_{us}(t)$ for each live-bed scour test.

The scour process downstream of the weir is recorded by datasets $X_6(t) \sim X_{40}(t)$. For each live bed test, the evolution of maximum scour depth downstream of the weir, $d_s(t)$, was extracted from datasets $X_6(t) \sim X_{40}(t)$ as $d_s(t) = -M\text{in}[X_6(t) \sim X_{40}(t)]$. Fig. 7 shows an example of the scour process downstream of the weir. The average equilibrium value, d_{s_a}, and the maximum value, $d_{s\_\max}$, of data series $d_s(t)$ were extracted for each live-bed scour test. Table 2 summaries the extracted values for each test.

Results and Discussion

Scour Mechanism

The clear-water scour equilibrium is defined as the condition when the scour hole dimensions do not change with time (Melville and Chiew 1999). Because of flume size limitation and the long duration of clear-water scour, only six clear-water scour tests were undertaken for this study. Under clear-water scour conditions, a small scour hole was observed at the upstream base of the weir. This scour hole was produced by weak vortices, generated by the interaction of the approach flow and the associated back flow. The temporal development of maximum scour depth downstream of the weir has three stages: (1) initial fast stage, (2) progressing stage, and (3) equilibrium stage (Guan et al. 2014).

Under live-bed scour conditions, the scour occurs both upstream and downstream of the weir, and sediment transport processes are highly influenced by excessive turbulence in the vicinity of the submerged weir. Strong downflows and secondary flows are generated at the upstream face of the weir when a bedform trough is approaching the weir upstream face. The downflow interacts with the main flow to create principal vortices, which cause the scour process upstream of the weir. The secondary flows alter the directions of the rotational axes of the principal vortices, resulting in helical motions of sediment in the scour hole. In general, these helical motions move laterally from bottom to top in the frontal zone of the weir upstream face. As these motions move to the weir top edge, the sediment is entrained by the main flow as suspended load, and is injected into the downstream scour hole.

A flow separation zone forms on the leeside of the dune, when the flow passes over a dune crest. Connected with the separation zone is a turbulent free shear layer, creating large scale eddies that travel through the flow domain and toward the surface while dissipating (Stoesser et al. 2008). Therefore, it can be inferred that periodic interactions of the large scale eddies in the dune trough and the helical vortices at the upstream base of the weir, cause the occurrence of scour-and-fill process immediately upstream of the weir.

Sediment transport over the weir occurs as suspended load, being entrainment by the accelerating flow on the crest of the weir. Near the weir, and in the scour holes, sediment moves as both suspended load and bed load. The maximum scour depth downstream of the weir is attained within a very short time, and then fluctuates around a mean depth in response to bedform migration.

As illustrated in Fig. 8, the flow regime over the weir transitions from a surface-flow regime to an impinging jet flow regime as the approach flow rate increases to a weir-height dependent threshold. According to previous studies (Wu and Rajaratnam 1996, 1998; Ohtsu et al. 1997), the flow regimes are dependent on the head difference across the weir and the approach flow rate. Because the tailwater depth is controlled to be a constant level in this study, the head difference across the weir is influenced only by weir height and flow rate (or intensity). Experimental results indicate that the transition stage (breaking wave or surface jump regime) between the surface-flow regime and the impinging-jet regime occurs at a value of the parameter $\alpha = (U_0/U_c)(z/h_t)^{0.2} \approx 1.45$. For the surface-flow regime ($0 \le \alpha \le 1.45$), the flow remains as a surface jet downstream of the submerged weir, and the scour hole downstream of the weir forms due to the increasing jet thickness and turbulence mixing with the tailwater [Figs. 7(a–c)]. For the impinging-jet regime ($\alpha > 1.45$), the flow plunges towards the bed, diffusing as a plane submerged jet, impacting the downstream bed, and inducing scour downstream of the weir [Fig. 8(d)].

Dimensionless Analysis of Local Scour

The geometry of the submerged weir under live-bed scour conditions is sketched in Fig. 1. The main parameters that determine the scour depth around the weir are

Table 2. Summary of Processed Experimental Results

Test number	Δt (s)	c (mm/s)	T (s)	λ (m)	η (mm)	η/λ	d_{s_a} (mm)	$d_{s\_\max}$ (mm)	d_{su_a} (mm)	$d_{su\_\max}$ (mm)
SCS4PO6.4	—[a]	—[a]	—[a]	—[a]	—[a]	—[a]	0	—[a]	—[a]	—[a]
SCS5PO12	—[a]	—[a]	—[a]	—[a]	—[a]	—[a]	165	18	—[a]	—[a]
SLSP12	832	0.24	4565	1.10	17	0.015	65	92	19	43
NLS1P13	647	0.31	3788	1.17	35	0.030	60	83	44	75
NLS2P15	344	0.58	1861	1.08	41	0.038	55	97	72	142
NLS3P17	263	0.76	1360	1.03	45	0.044	52	93	84	134
NLS4P19	164	1.22	824	1.00	48	0.048	51	92	87	132
NLS5P21	118	1.69	598	1.01	53	0.052	51	90	98	155
NLS6P23	77	2.60	416	1.08	56	0.052	60	107	111	162
NLS7P25	50	4.00	269	1.08	50	0.046	66	112	107	170
NLS8P27	31	6.45	169	1.09	47	0.043	74	114	107	174
NLS9P29	30	6.67	148	0.99	44	0.045	83	122	88	151
SLSP31	31	6.38	128	0.82	36	0.044	93	123	86	141
SLSP33	28	7.14	122	0.87	37	0.042	104	130	89	149
SLSP35	24	8.33	118	0.98	35	0.036	120	153	85	141
SLSP37	22	9.09	120	1.09	38	0.035	135	168	84	144
SLSP39	—[b]	—[b]	—[b]	—[b]	—[b]	—[b]	140	174	83	124
SCS0PO6	—[a]	—[a]	—[a]	—[a]	—[a]	—[a]	0	—[a]	—[a]	—[a]
SCS1P5.8	—[a]	—[a]	—[a]	—[a]	—[a]	—[a]	151	20	—[a]	—[a]
SCS2P7.5	—[a]	—[a]	—[a]	—[a]	—[a]	—[a]	196	26	—[a]	—[a]
SLSP12	868	0.23	4725	1.09	15	0.014	95	109	26	46
NLS10P13	670	0.30	4263	1.27	30	0.024	74	113	42	91
NLS11P15	401	0.50	2027	1.01	41	0.041	71	113	72	143
NLS12P17	264	0.76	1323	1.00	43	0.043	69	113	75	139
NLS13P19	182	1.10	995	1.09	50	0.046	68	116	88	140
NLS14P21	127	1.57	719	1.13	51	0.045	76	121	92	148
NLS15P23	86	2.33	530	1.23	57	0.046	84	122	93	153
NLS16P25	77	2.60	467	1.21	53	0.044	94	131	101	178
NLS17P27	46	4.35	268	1.17	47	0.040	110	142	90	181
SLSP29	39	5.16	169	0.87	35	0.040	122	149	84	134
SLSP31	33	6.15	135	0.83	35	0.042	152	172	76	146
SLSP33	28	7.27	104	0.76	31	0.041	168	202	75	140
SLSP35	24	8.42	98	0.83	34	0.041	189	212	77	107
SLSP37	—[b]	—[b]	—[b]	—[b]	—[b]	—[b]	198	226	73	119
SCS5PO5.6	—[a]	—[a]	—[a]	—[a]	—[a]	—[a]	0	—[a]	—[a]	—[a]
SLS1P12	888	0.23	4134	0.93	16	0.017	119	135	13	30
NLS18P13	707	0.28	4066	1.15	25	0.022	97	143	33	75
NLS19P15	540	0.37	2751	1.02	35	0.034	94	134	52	107
NLS20P17	347	0.58	1688	0.97	45	0.046	87	117	73	137
NLS21P19	230	0.87	1263	1.10	53	0.048	85	120	77	138
NLS22P21	143	1.40	824	1.15	54	0.047	92	125	86	130
NLS23P23	105	1.90	667	1.27	57	0.045	105	147	85	142
SLS7P24	91	2.21	517	1.14	53	0.046	135	161	90	147
NLS24P25	68	2.94	425	1.25	56	0.045	144	185	87	163
NLS25P27	47	4.26	262	1.11	51	0.046	169	204	82	147
SLS9P28	48	4.17	237	0.99	44	0.045	193	239	91	130
SLS10P29	40	5.00	183	0.92	42	0.046	205	246	84	114
SLS11P30	34	5.88	158	0.93	42	0.045	226	251	83	115

[a]Not applicable for clear-water scour conditions.
[b]Developed data process method is out of effect at bedform transition regime.

$$y = f(\rho, \nu, g, h_0, h_t, U_0, \rho_s, d_{50}, \sigma_g, U_c, b, z) \tag{1}$$

where y = scour depth parameter (d_{us_a}, d_{s_a}); ν = fluid kinematic viscosity; g = acceleration of gravity; ρ, ρ_s are the densities of water and sediment, respectively; b = weir width; and z = weir height. Eq. (1) includes a consideration of approach flow and tailwater conditions ($\rho, \nu, g, h_0, h_t, U_0$), sediment characteristics and transport ($\rho_s, d_{50}, \sigma_g, U_c$), and structure geometry (b, z).

In this study, sediment and weir width have been kept constant. Because a controlled tailwater depth was used, the approach flow depth is dependent on the flow intensity and weir height. Thus, assuming constant relative density of sediment and fluid viscosity, a dimensionless expression for the equilibrium scour depth around the submerged weir in a uniform sediment can be developed from Eq. (1)

$$\frac{y}{h_t} = f\left(\frac{U_0}{U_c}, \frac{z}{h_t}\right) \tag{2}$$

In this study, the ranges for the flow intensity and normalized weir height are $1.0 \leq U_0/U_c \leq 3.1$ and $0.2 \leq z/h_t \leq 0.33$, respectively.

Scour Upstream of the Weir

The normalized upstream average maximum scour depth, d_{us_a}/h_t, as a function of flow intensity, U_0/U_c, is shown in Fig. 9. Under the

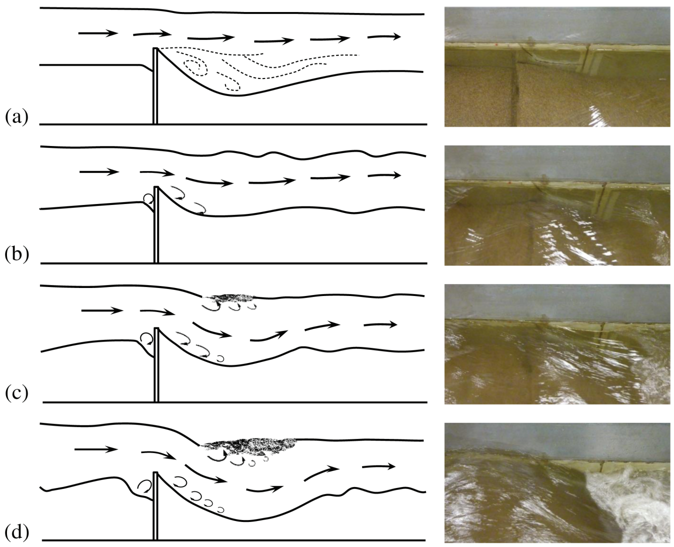

Fig. 8. (Color) Flow regimes passing over the weir: (a) surface jet; (b) surface wave; (c) transition stage (breaking wave or surface jump); (d) impinging jet (image by Dawei Guan)

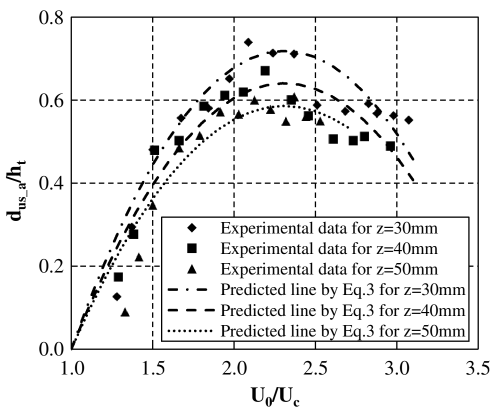

Fig. 9. Normalized upstream average maximum scour depth versus flow intensity

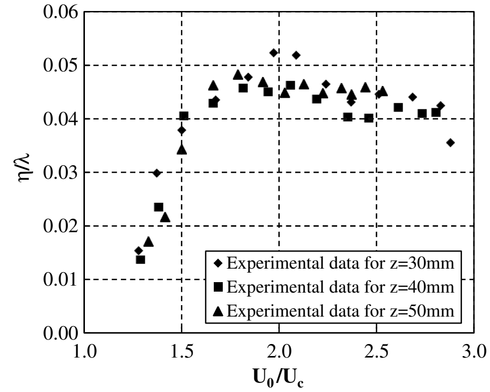

Fig. 10. Bedform steepness versus flow intensity

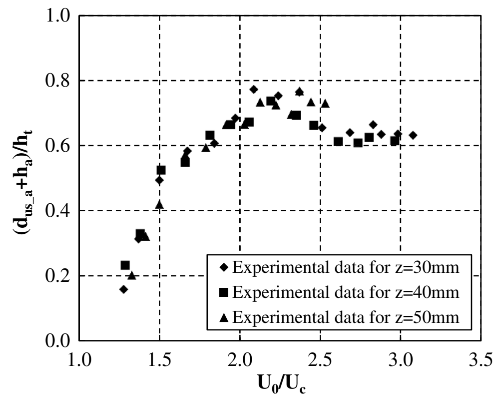

Fig. 11. Adjusted normalized upstream average maximum scour depth (by aggradation height) versus flow intensity

live-bed scour conditions, the scour-and-fill process upstream of the weir is induced by approaching periodic bedforms. For each weir height, the normalized scour depth has an increasing trend for U_0/U_c between 1.2 and 2.2, and then decreases as U_0/U_c increases further. A parallel plot of bedform steepness, η/λ, against U_0/U_c is shown in Fig. 10. Bedform steepness is found to be independent of weir height, as expected. The developing trends in Figs. 9 and 10 clearly show that bedform steepness has a strong correlation with the inducement of the scour-and-fill process upstream of the weir. Fig. 9 also shows that d_{us_a}/h_t decreases as the weir height increases. This is because of aggradation in the approach flow. For higher weir heights, the aggradation height has larger values for the same flow intensity conditions (Table 2), thereby decreasing d_{us_a}. The scour depths for the three different weir heights in Fig. 9 overlap if d_{us_a} is expressed in terms of upstream equilibrium bed level, as shown in Fig. 11. In this study, the aggradation height is found to be dependent on the approach flow depth, flow rate and weir height, which have been included in Eq. (1). Therefore the effect of aggradation on scour upstream of weir has been implicitly accounted for in the previous dimensional analysis [Eq. (2)].

As seen from Fig. 9, a parabolic relationship between d_{us_a}/h_t and U_0/U_c can be adopted. Assuming d_{us_a}/h_t starts at $U_0/U_c = 1$, the following numerical form of Eq. (2) is derived from the experimental data:

$$\frac{d_{us\_a}}{h_t} = 0.22\left(\frac{z}{h_t}\right)^{-0.40}\left(\frac{U_0}{U_c}-1\right)\left(3.62-\frac{U_0}{U_c}\right) \tag{3}$$

Eq. (3) is valid for $1.0 \le U_0/U_c \le 3.1$ with a multiple correlation coefficient $R^2 = 0.85$ and the mean relative deviation MRD = 0.156. Eq. (3) is plotted in Fig. 9 for the three different weir heights, fitting the existing experimental data. Because of insufficient experimental data, the magnitude of the scour depth upstream of the weir under clear water conditions ($0 \le U_0/U_c < 1$) is not discussed in this study.

Considering that the scour-and-fill process upstream of the weir is induced by approaching bedforms, the normalized upstream average maximum scour depth can also be expressed as

$$\frac{d_{us\_a}}{h_t} = f\left(\frac{\eta}{\lambda}, \frac{z}{h_t}\right) \tag{4}$$

As shown in Figs. 9 and 11, the weir height effect can be eliminated by adding the average aggradation height to the average maximum scour depth. As shown in Eq. (3), the $(z/h_t)^{-0.40}$ term accounts for the aggradation effect. Therefore, Eq. (4) can be simplified as

$$\frac{d_{us\_a}}{h_t}\left(\frac{z}{h_t}\right)^{0.40} = f\left(\frac{\eta}{\lambda}\right) \tag{5}$$

The values for $(d_{us\_a}/h_t)(z/h_t)^{0.4}$ and η/λ are plotted in Fig. 12. The trend suggests an exponential relationship between the adjusted normalized scour depth and bedform steepness, leading to

$$\frac{d_{us\_a}}{h_t} = 20.85\left(\frac{z}{h_t}\right)^{-0.40}\left(\frac{\eta}{\lambda}\right)^{1.32} \tag{6}$$

for which the correlation coefficient is $R^2 = 0.87$ and mean relative deviation is MRD = 0.104.

Scour Downstream of the Weir

The normalized value of the scour depth downstream of the weir, d_{s_a}/h_t, as a function of flow intensity, U_0/U_c, is illustrated in Fig. 13. It can be seen that the scour depth downstream of the weir increases as the weir height increases. For each weir height, the experimental data show that the normalized scour depth reaches a peak at the transition ($U_0/U_c = 1$) from clear-water scour to live-bed scour conditions. A significant drop occurs just beyond reaching the peak, with another increase after reaching its minimum.

Because of insufficient data for clear-water scour conditions in this study, a linear relationship is assumed between the maximum scour depth downstream of the weir and both flow intensity and weir height. Based on this assumption and Eq. (2), the equilibrium clear-water scour depth, denoted by d_{s_a}, can be expressed by Eq. (7)

$$\frac{d_{s\_a}}{h_t} = 2.76\frac{U_0}{U_c} + 1.90\frac{z}{h_t} - 1.81 \tag{7}$$

Eq. (7) has a multiple correlation $R^2 = 0.99$ and is valid for $U_0/U_c < 1$. Its lower limit of validity is $U_0/U_c \approx 0.5$. This is because the scour downstream of the weir starts at $U_0/U_c \approx 0.5$ rather than $U_0/U_c = 0$ (Fig. 13). The exact value depends on weir height. Therefore, d_{s_a} should be considered to be zero when a negative value of scour depth results from using Eq. (7).

For live-bed scour conditions ($U_0/U_c > 1$), the normalized downstream scour depth d_{s_a}/h_t decreases to its minimum value, then increases again with the increase of flow intensity U_0/U_c, for each weir height. It is observed that the minimum scour depths occur almost at the transition from the surface-flow regime to the impinging-jet regime (Fig. 13). As explained above, the impinging-jet regime has a direct impact on the downstream bed, and it can induce a larger erosive force in the scour hole than the scour mechanism under the surface-flow regime.

The equilibrium scour depth downstream of the weir is a balance between the upstream sediment supply rate and scour rate in the scour hole. For the surface-flow regime under live-bed scour conditions ($U_0/U_c = 1 \sim 1.5$) and increasing flow rate, the upstream sediment supply rate and the scour rate are both increasing and the upstream sediment supply rate is larger than the scour rate. The rate of sediment supply increase is less than the rate of increase of scour, resulting in a decreasing trend in the scour depth and a minimum near the transition from the surface-flow regime to the impinging-jet regime. As flow conditions change to the impinging-jet regime, the scour rate becomes increasingly larger than the upstream sediment supply rate, resulting in the observed trend of scour depth downstream of the weir. Based on the experimental data and Eq. (2), the following Eqs. (8) and (9) are derived for live-bed scour under the surface-flow regime and the impinging jet flow regimes, respectively:

$$\frac{d_{s\_a}}{h_t} = 5.42\left(\frac{U_0}{U_c}\right)^{-9.87}\left(\frac{z}{h_t}\right)\exp\left[5.76\left(\frac{U_0}{U_c} - 1\right)\right] \quad \text{(surface-flow regime)} \tag{8}$$

$$\frac{d_{s\_a}}{h_t} = 0.76\left(\frac{U_0}{U_c}\right)^{2.27}\left(\frac{z}{h_t}\right)^{1.46} \quad \text{(impinging-jet regime)} \tag{9}$$

Eq. (8) is valid for $1 \leq U_0/U_c < 1.45(z/h_t)^{-0.2}$. The multiple correlation coefficient is $R^2 = 0.98$ and mean relative deviation is MRD = 0.048. Eq. (9) is only valid for $1.45(z/h_t)^{-0.2} \leq U_0/U_c \leq 2.5$ due to insufficient data for weir height 50 mm and for higher U_0/U_c. The multiple correlation coefficient is $R^2 = 0.97$ and mean relative deviation is MRD = 0.061. Eqs. (7)–(9) are also plotted in Fig. 13 for the three different weir heights. The plots of the equations fit the experimental data.

For live-bed scour at piers or abutments, a similar trend occurs. Scour depth initially reduces with increase in approach flow velocity, reaches a minimum value, and then increases again toward a second maximum. The second maximum occurs at about the transitional flat-bed stage of sediment transport on the channel bed and is termed the live bed peak (Melville 1984, 1992). Although Fig. 13 shows a similar trend to that for scour at piers and abutments, whether the scour depth downstream of the weir reaches a live bed

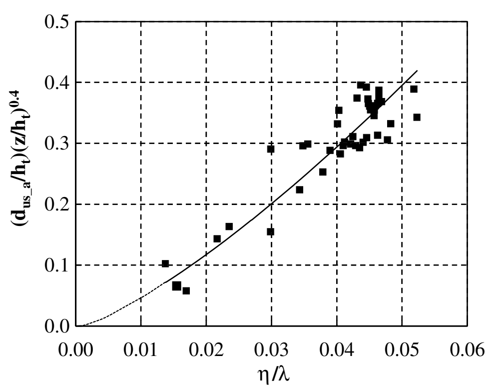

Fig. 12. Upstream average maximum scour depths versus bedform steepness

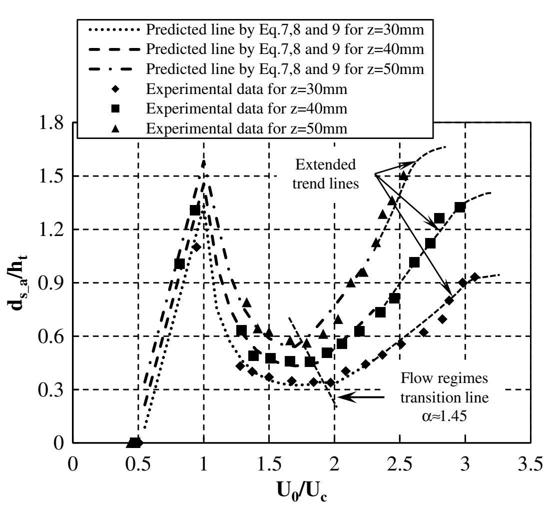

Fig. 13. Normalized scour depth downstream of the weir as a function of flow intensity

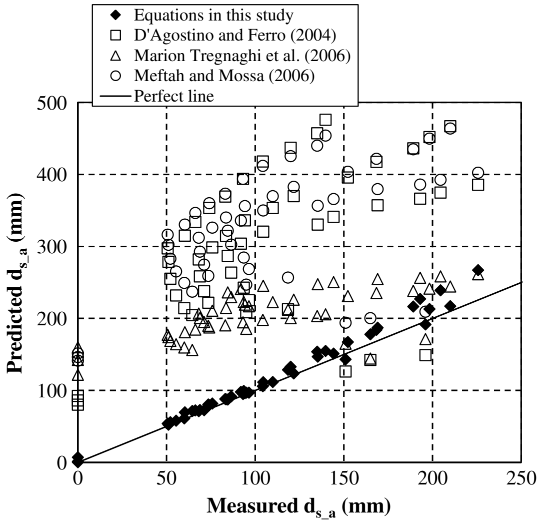

Fig. 14. Comparison between measured equilibrium scour depth (downstream) and predicted values by equations in this study and equations from literature

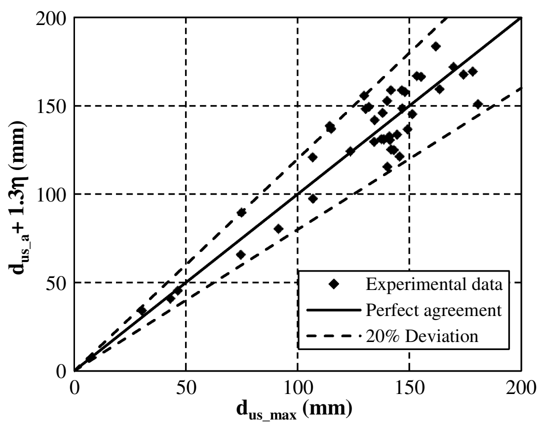

Fig. 15. Comparison of observed maximum scour depths versus adjusted average maximum scour depths upstream of the weir (by bedform height)

peak at higher flow intensities (bedform plane bed stage and antidune stage) is still unknown because of different scour mechanisms and the limitation of the flume capacity and the different scour mechanisms in this study. However, it is most likely that the normalized scour depth will attain a second peak at very high flow intensities (Fig. 13).

A comparison between measured equilibrium scour depth, d_{s_a}, and predicted values by Eqs. (7)–(9) and equations found in the literature (D'Agostino and Ferro 2004; Ben Meftah and Mossa 2006; Marion et al. 2006) is shown in Fig. 14. There is no weir spacing effect in this study, thus the distance between two sequent weirs is assumed to be infinity. The morphological jump "a_1" in Marion et al. (2006) and the product "LS_0" in Ben Meftah and Mossa (2006) are taken as the weir height z in this study. As seen in Fig. 14, the equations found in the literature greatly overestimate the equilibrium scour depth downstream of the weir for most of cases. The most important reasons are that their equations were developed for the unsubmerged weirs or sills and excluded the upstream bedform influence.

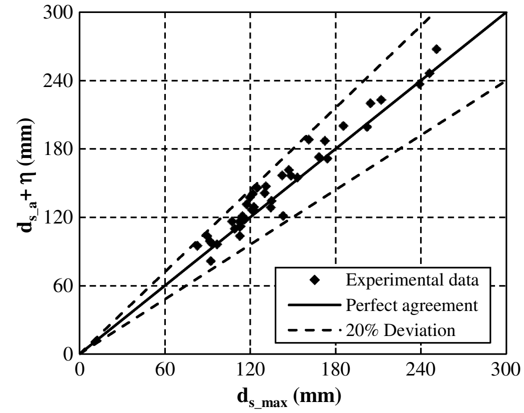

Fig. 16. Comparison of observed maximum scour depths versus adjusted average scour depths downstream of the weir (by bedform height)

For design purposes, the maximum scour depth at both sides of the weir should be considered as the principal parameter. Therefore, a relationship between the maximum scour depth and average maximum scour depths is needed. From perusal of all the results for live-bed scour conditions (Table 2), it was observed that the maximum scour depth both upstream and downstream of the weir can be approximated as the summation of average maximum scour depth and a multiple of bedform height

$$d_{us\_\max} \approx (d_{us\_a} + 1.3\eta) \tag{10}$$

$$d_{s\_\max} \approx (d_{s\_a} + \eta) \tag{11}$$

The values for $[d_{us\_\max}, (d_{us\_a} + 1.3\eta)]$ and $[d_{s\_\max}, (d_{s\_a} + \eta)]$ are plotted in Figs. 15 and 16, respectively. All the plotted points are within ±20% deviation of the perfect agreement line.

Conclusions

Live-bed scour at submerged weirs was experimentally studied. The challenging noisy measurement environment was overcome by applying a data-processing technique, whereby scour data and bedform information are extracted from highly contaminated bed elevation data. The experimental data are limited to rectangular weirs in uniform sand beds.

Under live-bed conditions, a scour-and-fill process occurs immediately upstream from the weir due to periodic approaching bedforms. The average maximum scour depths upstream of the weir are found to be strongly dependent on flow intensity and the steepness of the approaching bedforms. Eqs. (3) and (6) are developed for the prediction of the average maximum scour depths upstream of the weir.

For the scour process downstream of the weir, a multiple linear relationship [Eq. (7)] between normalized equilibrium scour depth, flow intensity and normalized weir height is derived for clear-water scour conditions. For live-bed scour downstream of the weir, the scour mechanism changes as the flow regime over the weir transitions from the surface-flow regime to the impinging-jet regime. The transition stage between surface-flow regime and impinging-jet regime occurs at $\alpha = (U_0/U_c)(z/h_t)^{0.2} \approx 1.45$. Under surface-flow regimes, the scour process is due to downstream-increasing jet thickness and turbulence mixing with the tailwater. Under impinging-jet regimes, the downstream scour process is caused by jet diffusion and direct impact forces from the jet impinging on the bed. Two live-bed scour equations [Eqs. (8) and (9)] are proposed for predicting equilibrium scour depth downstream of the submerged weir under surface-flow regimes and impinging-jet regimes, respectively.

For the live-bed scour conditions, the maximum scour depth both upstream and downstream of the weir is approximately equal to the summation of average maximum scour depth and a multiple of bedform height.

Acknowledgments

The authors would like to thank China Scholarship Council (CSC) for the financial support of this research. Also, the valuable suggestions from Dr. Keith Adams are appreciated.

Notation

The following symbols are used in this paper:

b = weir width;
c = bedform celerity;
d_{50} = median diameter of sediment;
d_{s_a} = average value of $d_s(t)$ (also taken as equilibrium scour depth for clear-water scour);
$d_{s\_\max}$ = maximum value of $d_s(t)$;
$d_s(t)$ = maximum scour depth downstream of the weir at time t;
d_{us_a} = average maximum scour depth upstream of the weir (average value of d_{us_sf});
$d_{us\_\max}$ = maximum value of $d_{us}(t)$;
d_{us_sf} = maximum scour depth for each scour-and-fill process;
$d_{us}(t)$ = maximum scour depth upstream of the weir at time t;
$E[\,]$ = function for the expected value;
F_u = Froude number upstream of the weir;
g = acceleration of gravity;
H_d = water level difference across the weir;
h_a = aggradation height;
h_0 = average approach flow depth;
h_t = tail water depth;
i = transducer number ($i = 1 \sim 40$);
L = distance between Transducers 1 and 2;
$\mathrm{Max}[\,]$ = function for maximum value;
$\mathrm{Min}[\,]$ = function for minimum value;
MRD = mean relative deviation;
m = total number of counted bedforms;
n = total number of counted bedform crests and troughs;
Q = flowrate;
$R_{x_1x_2}$ = cross-correlation function;
R^2 = correlation coefficient;
S = flume slope;
T = average bedform period;
t = scour time;
$t(n)$ = time for the points (where bedform crests or troughs pass Transducer 1) extracted from dataset $X_1(t)$;
$t_p(m)$ = serial bedform periods;
U_c = critical average approach flow velocity;
U_0 = average approach flow velocity;
u_{*c} = average approach flow critical shear velocity;
$X_i(t)$ = filtered time-series dataset for transducer i;
y = scour depth parameter (d_{us_a}, d_{s_a});
z = weir height;
α = parameter for determining flow regime;
Δ = relative submerged particle density;
Δt = time delay;
η = bedform heights;
$\eta(m)$ = serial bedform heights;
λ = average bedform length;
ν = kinematic viscosity of fluid;
ρ = water density;
ρ_s = sediment density;
σ_g = standard deviation of sediment size; and
$\sim$ = connection sign for values in a range or that are related.

References

Ben Meftah, M., and Mossa, M. (2006). "Scour holes downstream of bed sills in low-gradient channels." *J. Hydraul. Res.*, 44(4), 497–509.

Bhuiyan, F., Hey, R. D., and Wormleaton, P. R. (2009). "Effects of vanes and W-Weir on sediment transport in meandering channels." *J. Hydraul. Eng.*, 10.1061/(ASCE)0733-9429(2009)135:5(339), 339–349.

Bormann, N. E., and Julien, P. Y. (1991). "Scour downstream of grade-control structures." *J. Hydraul. Eng.*, 10.1061/(ASCE)0733-9429(1991)117:5(579), 579–594.

Comiti, F., Andreoli, A., and Lenzi, M. A. (2005). "Morphological effects of local scouring in step-pool streams." *Earth Surf. Processes Landforms*, 30(12), 1567–1581.

Comiti, F., Cadol, D., and Wohl, E. (2009). "Flow regimes, bed morphology, and flow resistance in self-formed step-pool channels." *Water Resour. Res.*, 45(4), W04424.

Comiti, F., and Lenzi, M. A. (2006). "Dimensions of standing waves at steps in mountain rivers." *Water Resour. Res.*, 42(3), W03411.

D'Agostino, V., and Ferro, V. (2004). "Scour on alluvial bed downstream of grade-control structures." *J. Hydraul. Eng.*, 10.1061/(ASCE)0733-9429(2004)130:1(24), 24–37.

Friedrich, H. (2010). "Evaluation of statistical analysis techniques for developing bedforms recorded in 3D." Ph.D. thesis, Univ. of Auckland, New Zealand.

Friedrich, H., Melville, B. W., Coleman, S. E., Nikora, V. I., and Clunie, T. M. (2005). "Three-dimensional measurement of laboratory submerged bed forms using moving probes." *Proc., XXXI IAHR Congress*, Korea Water Resources Association, Seoul, Korea, 396–404.

Gaudio, R., Marion, A., and Bovolin, V. (2000). "Morphological effects of bed sills in degrading rivers." *J. Hydraul. Res.*, 38(2), 89–96.

Guan, D., Melville, B., and Friedrich, H. (2014). "Flow patterns and turbulence structures in a scour hole downstream of a submerged weir." *J. Hydraul. Eng.*, 10.1061/(ASCE)HY.1943-7900.0000803, 68–76.

Lenzi, M. A., Marion, A., and Comiti, F. (2003a). "Interference processes on scouring at bed sills." *Earth Surf. Processes Landforms*, 28(1), 99–110.

Lenzi, M. A., Marion, A., and Comiti, F. (2003b). "Local scouring at grade-control structures in alluvial mountain rivers." *Water Resour. Res.*, 39(7), 1176.

Marion, A., Lenzi, M. A., and Comiti, F. (2004). "Effect of sill spacing and sediment size grading on scouring at grade-control structures." *Earth Surf. Processes Landforms*, 29(8), 983–993.

Marion, A., Tregnaghi, M., and Tait, S. (2006). "Sediment supply and local scouring at bed sills in high-gradient streams." *Water Resour. Res.*, 42(6), W06416.

Melville, B. W. (1984). "Live-bed scour at bridge piers." *J. Hydraul. Eng.*, 10.1061/(ASCE)0733-9429(1984)110:9(1234), 1234–1247.

Melville, B. W. (1992). "Local scour at bridge abutments." *J. Hydraul. Eng.*, 10.1061/(ASCE)0733-9429(1992)118:4(615), 615–631.

Melville, B. W. (1997). "Pier and abutment scour: Integrated approach." *J. Hydraul. Eng.*, 10.1061/(ASCE)0733-9429(1997)123:2(125), 125–136.

Melville, B. W., and Chiew, Y. (1999). "Time scale for local scour at bridge piers." *J. Hydraul. Eng.*, 10.1061/(ASCE)0733-9429(1999)125:1(59), 59–65.

Ohtsu, I., Yasuda, Y., and Yamanaka, Y. (1997). "Discussion of 'Submerged flow regimes of rectangular sharp-crested weirs' by S. Wu and N. Rajaratnam." *J. Hydraul. Eng.*, 10.1061/(ASCE)0733-9429(1997)123:10(927.2), 927–929.

Pagliara, S., and Kurdistani, S. M. (2013). "Scour downstream of cross-vane structures." *J. Hydro-environ. Res.*, 7(4), 236–242.

Sheppard, D. M., and Miller, W. (2006). "Live-bed local pier scour experiments." *J. Hydraul. Eng.*, 10.1061/(ASCE)0733-9429(2006)132:7(635), 635–642.

Stoesser, T., Braun, C., García-Villalba, M., and Rodi, W. (2008). "Turbulence structures in flow over two-dimensional dunes." *J. Hydraul. Eng.*, 10.1061/(ASCE)0733-9429(2008)134:1(42), 42–55.

Wu, S., and Rajaratnam, N. (1996). "Submerged flow regimes of rectangular sharp-crested weirs." *J. Hydraul. Eng.*, 10.1061/(ASCE)0733-9429(1996)122:7(412), 412–414.

Wu, S., and Rajaratnam, N. (1998). "Impinging jet and surface flow regimes at drop structures." *J. Hydraul. Res.*, 36(1), 69–74.